The initiation of pull-apart basins and transform continental margins: results from numerical experiments of kinematic partitioning in divergent settings

Christophe Basile, Jean Braun

The initiation of pull-apart basins and transform continental margins: results from numerical experiments of kinematic partitioning in divergent settings

Christophe Basile and Jean Braun

Address: Université Grenoble Alpes, ISTerre, F-38041, France
christophe.basile@ujf-grenoble.fr; jean.braun@ujf-grenoble.fr

Abstract

We present a set of numerical models to investigate how transform faults initiate in pull-apart-basins or transform continental margins. The model represents an elastic plate with three aligned weak spots. Applying strain on the edge of the model firstly propagate extensional cracks from the preexisting damaged spots. The subsequent evolution depends on the angle (obliquity) between the applied strain and the alignment of the damaged spots. For obliquity < 50°, transform faults appear to connect en-échelon divergent cracks; for obliquity > 60°, transtensional transfer zones connect the divergent cracks and no transform fault forms. These experiments suggest that pull-apart basins do not form as previously assumed by connection of overlapping transform faults, but that transform faults appear as connections of extensional areas.

Keywords: pull-apart basin, transform margin, transfer fault, oblique margin

Introduction

Among sedimentary basins found in the vicinity of strike-slip faults, pull-apart basins are "located between two overlapping en-échelon strike-slip faults terminations" (Aydin and Nur, 1982) (Figure 1a). A right-lateral step-over pulls apart the overlapping area during dextral strike-slip movement (Figure 1a). A similar setting is observed along oceanic accretion axes, where oceanic spreading centres alternate with transform faults, and along continental margins with alternating divergent and transform margins.

How such structures develop remains a long-standing, and still unsolved problem. The main proposed hypothesis is that strike-slip faults are located on inherited structures (Wilson, 1965; Sibuet and Mascle, 1978; Dooley et al., 1999; Bellahsen et al., 2013) (Figure 2a). This hypothesis is supported by the fact that tensional overlaps never appear along incipient strike-slip fault. A newly created strike-slip fault first develops en-échelon Riedel faults separated

by compressional overlaps, dextral strike-slip generating left-lateral en-échelon Riedel faults (Cloos, 1928; Riedel, 1929; Tchalenko, 1970). As a consequence, most analogue modelling (e.g. Hempton and Neher, 1986; Dooley and McClay, 1997; Rahe et al., 1998; Basile and Brun, 1999) and numerical modelling (Segall and Pollard, 1980; Petrunin and Sobolev, 2008) efforts consider an en-échelon disposition of strike-slip fault segments as a starting configuration, and investigate how the two tips of the faults interfere to form a pull-apart basin.

However, a new concept recently emerged from studies of the oceanic domain. Based on a detailed structural analysis of the back-arc Woodlark basin, Taylor et al. (2009) concluded that transform faults were absent during the rifting stage, and appeared to connect spreading axis after the oceanic accretion started (Figure 2b).

Using different assumptions, several numerical models supported this assumption that oceanic transform faults may not be inherited. Hyeronimus (2004) and Gerya (2013a and b) proposed that pull-apart step-overs result from the linkage of divergent domains by strike-slip faults. Gerya (2010) also proposed that crenelated oceanic transform faults (type II of Turcotte, 1974) may result from dynamical instabilities of propagating oceanic accretion axis.

Because Hyeronimus (2004) models are based on the deformation of an elastic plate, they are not specific to the oceanic lithosphere, and their results may be applicable to both continental and oceanic plates. Using this approach, we investigate here the kinematic conditions necessary for the formation of transform faults between propagating divergent plate boundaries.

Kinematic partitioning

The key parameter we test here is the regional obliquity between the plate boundary orientation and the kinematic displacement. To illustrate what is meant here, let's consider a typical oceanic spreading axis composed of alternating transform and divergent plate boundary segments (type I of Turcotte, 1974; Figure 1). The regional trend of the plate boundary is defined by the alignment of transform-divergent segment intersections, and the obliquity by the angle between this alignment and the relative displacement between the two plates, assumed to be parallel to the transform faults (Figure 1) (Basile, 2015). When adjacent transform and divergent plate boundaries are perpendicular, the obliquity can also be defined from the ratio between the lengths of adjacent divergent and transform boundaries (Figure 1b).

The obliquity may vary from 0° (pure transform fault: displacement parallel to the plate boundary) to 90° (pure divergent plate boundary, perpendicular to the plate displacement). Between these two extreme values, the obliquity is accommodated by spatial partitioning of the deformation among alternating transform and divergent plate boundary segments. The transform segments are longer for obliquity lower than 45°, while divergent segments are longer for obliquity higher than 45° (Basile, 2015).

Obliquity can be defined in a similar way for continental margins by considering the intersections of transform and divergent margin segment (Figure 1b), or for pull-apart basins by the edges of successive basins separated by strike-slip faults (Figure 1a). For example, in the Equatorial Atlantic Ocean, the obliquity vary from 5 to 20° in the Romanche and Saint Paul fracture zones, and from 50° to 80° between the Saint Paul and Doldrums fracture zones (Figure 1c).

Methodology

We use the elastic plate model described in Hieronymus (2004), based on Pollard and Aydin (1984). We refer the reader to Hieronymus (2004) and the supplementary material for a full description of the model. Hieronymus (2004) described how the deformation is controlled by the model parameters in a given kinematic setting. Here, we investigate how the orientation of the applied strain controls the deformation pattern.

We use a finite element approximation on a 101x101–nodes two-dimensional grid where damaged weak zones have been embedded to localise deformation. Damage evolution is described by a tensile damage coefficient, θ_1 that affects both bulk and shear modulus, and a shear damage coefficient, θ_2 that affects only the shear modulus.

Initially, three weak zones are aligned in the middle part of the grid, and a divergent displacement field strain is applied on the top and bottom edges of the grid (Figure 3). To avoid or at least minimise the development of edge instabilities, periodic boundary conditions are imposed on the left and right boundaries, so that the solution (displacement, stress and damage parameters) are identical on these two edges.

Results

We first describe the evolution of a “reference” model where the obliquity, the angle between the applied left-lateral strain and the alignment of the damaged zones (Figure 4), is 40° . During the first stages of model evolution, the tensile strain decreases from the top and

bottom boundaries towards the model centre where the three damaged weak zones are located. En-échelon cracks rapidly develop between the damages zones, with a right-lateral step-over geometry (Figure 4g). The cracks initially trend at 55° relative to the applied strain (Figure 4a). As they propagate, they progressively rotate to become more perpendicular to the displacement direction, and their trend rapidly changes from 55° to 75° (Figure 4b). The propagation of the tensile cracks ends when damaged zones parallel to the displacement direction develop to connect the individual cracks (Figure 4c and 4e). At this stage, the strain is almost uniform in the intact part of the elastic plate on both sides of the damaged zone, which can be considered as a plate boundary consisting of alternating obliquely divergent and transform segments. This setting is stable, i.e. it does not evolve with increasing strain (Figure 4d and 4f).

Influence of obliquity on model evolution

Changing the obliquity leads to the development of four different patterns of deformation (Figure 5):

1. for low obliquities (0°: pure strike-slip, Figure 5a, or 10°, Figure 5b), the tensile cracks do not develop, and a single damaged zone forms by connecting the initially damaged spots. This damaged zone can be considered as a pure strike-slip fault, at least in the first stages of evolution when the damaged zone is parallel to the local strain. Increasing deformation widens the damaged zone, deformation is less localised, and instabilities develop around the initially damaged spots.

2. for a wide range of low to medium obliquities (from 20° -Figure 5c- to 50° -Figure 5f-), the deformation pattern consists of alternating transform faults and oblique divergent zones. In these model experiments tensile cracks connected by transform faults develop (Figure 5g). The angle between the tensile cracks and the applied strain decreases with the obliquity, from 75° for the experiments with 50°- and 40°-obliquity (Figure 5f and 5e), to 70° for 30°-obliquity (Figure 5d) and 55° for 20°-obliquity (Figure 5c). In all cases, the orientation of the transform boundaries develop parallel to the applied displacement direction. However, to develop the connections by transform faults requires higher total strain for the lower obliquities (20° and below), which is a simple consequence of the correspondingly greater length of transform faults.

3. for high obliquities (> 50°), connections between the tensile cracks do not develop parallel to the imposed displacement direction (Figures 5h to 5j for 60° to 80°-obliquity), but by transtensional relays (Figure 5k), whose length and strike-slip component decrease

as obliquity increases. The transtensional relays trend at 15° to the applied displacement direction for the 60°-obliquity experiment (Figure 5h), 30° for the 70°-obliquity experiment (Figure 5i) and 45° for the 80°-obliquity experiment (Figure 5j). The orientation of the tensile cracks also changes with the obliquity, increasing from 70° to 80° and 85° to the applied displacement direction in the 60°-, 70°- and 80°-obliquity experiments, respectively (Figure 5h to 5j).

4. for 90°-obliquity (Figure 5l), the damaged zone connects the initial spots to form a single band perpendicular to the applied strain, that can be interpreted as a single divergent plate boundary.

Discussion

The long-standing paradigm concerning the formation of pull-apart basins and alternating transform and divergent margin segments is that the basins form as a connection between overlapping transform faults (Wilson, 1965; Sibuet and Mascle, 1978; Segall and Pollard, 1980; Hempton and Neher, 1986; Dooley and McClay, 1997). This paradigm appeared to be in contradiction with the propagation of oceanic spreading axis (Hey, 1977), and more recently to observations (Taylor et al., 2009) and models (Hieronymus, 2004; Gerya 2010, 2013a) of formation of oceanic transform faults connecting spreading axis. The first and main result from the numerical experiments we present here is to extend this change of paradigm to continental setting (pull-apart basins) and continent-ocean boundaries (transform continental margins). Our experiments confirm that transform faults do initiate as connections between propagating divergent plate boundaries (Figure 4g). This explains the common occurrence of extensional overlaps in strike-slip settings, while strike-slip faulting alone always forms compressional overlaps between en-échelon Riedel faults. This change of paradigm implies that, as for divergent continental rifting (Dunbar and Sawyer, 1988), the main structural heritages controlling the location of an incipient oblique plate boundary are lithospheric weak zones where stretching localises. This does not exclude that inherited structures, such as older strike-slip faults or verticalized sutures, may also localise incipient transform faults between incipient divergent basins when they present the adequate orientation. The very low obliquity experiments (0 to 10°, Figure 5a and 5b) suggest that, in such settings, lithospheric weak zones can also localise transform faults.

Other important results are that the shape of the incipient plate boundary does not change linearly with the obliquity, and that transform faults do not form at high obliquity. Of course, 90°-obliquity leads to the formation of a pure divergent plate boundary, and 0°- and

10°-obliquity to pure transform fault. In between, the deformation always evolves by nucleation and propagation of extensional cracks from the inherited weak zones. However, the later connection between these extensional segments can occur in two ways. For obliquities in the range 20 to 50°, transform faults parallel to the imposed displacement direction form and connect extensional segments that accommodate a significant strike-slip component (Figure 5g). For obliquities higher than 60°, the extensional segments show very little strike-slip component but are connected by transtensional transfer zones. These transfer zones are not parallel to the strain, but accommodate a significant strike-slip component (Figure 5k). There therefore appears to be a threshold in obliquity separating two possible structural settings. The exact value of this threshold is controlled by the values of the parameters used in the model which are difficult to constrain, and are expected to vary in nature, depending, for example, on lithospheric type (oceanic or continental) and age. Consequently, although the existence of a threshold separating two radically different behaviors is likely to exist, its value and how it may vary with the structure of the lithosphere needs to be appropriately addressed by more sophisticated thermo-mechanical models, that can also take into account the vertical rheological layering of the lithosphere.

To address the question whether such a threshold separating two different behaviors exists in the natural world, we used M. Mercier de Lépinay et al.'s (unpublished data) compilation of 79 transform margins worldwide. Transform margins are mostly located in areas with low to medium regional obliquity, such as the Equatorial Atlantic or South East Africa. In these areas, the divergent margins are not perpendicular to the adjacent transform margins (e.g. Moulin et al., 2010 in the Equatorial Atlantic). As the plate displacement is assumed to be parallel to the transform faults, it implies that the motion along the rifted margin segments include a significant strike-slip component.

In continental margins that formed in high obliquity settings, such as the Central and South Atlantic oceans, very few transform margins are observed (M. Mercier de Lépinay et al., unpublished data). In these areas, extension have been accommodated by alternating rifted and transtensional segments, identified as transfer zones (Morley et al., 1990; Moy and Imber, 2009), oblique transfer zones (Bellahsen et al., 2013) or oblique-rifted margins (Mounguengui and Guiraud, 2009).

Both the geographical distribution of transform margin segments and the orientation of rifted margin segments relative to the orientation of transform segments suggest, as in the numerical experiments, a dual behavior in the localisation of deformation during continental

break-up. Transfer zones form between rift segments when the obliquity is high (≥60°), whereas transform faults form at lower obliquity (≤50°) between transtensional rifts.

In all the experiments where transform faults form between divergent segments, the localisation of deformation always first occurs in propagating divergent segments, then along the transform fault. This chronology may be compared with the incipient deformation of natural examples, as the Equatorial Atlantic. In this area, the oldest sediments found in some divergent basins are late Berriasian, more generally Barremian in age, while the older sediments associated with the onset of the Romanche transform fault are more recent, Aptian in age (Basile et al., 2005 and references herein). This supports the chronology shown by the experiments, even if this should not be used as a definite clue of the anteriority of divergent basins relatively to the transform ones, as transform faults only provide a poor stratigraphic record.

Conclusions

In oblique divergent plate tectonic settings, kinematic partitioning results in alternation of divergent and transform boundaries. This alternation defines the obliquity, i.e. the angle between the plate boundary and the relative motion between the two plates. Numerical experiments on the deformation of an elastic plate in which aligned weak zones have been embedded suggest that divergent boundaries or pull-apart basins do not form between transform faults, but, on the contrary, that transform faults initiate as connections between propagating divergent rift segments. However, transform faults only appear when the obliquity is less than 60°. For obliquities equal or higher than 60°, an oblique rift forms where individual rift segments are connected by transtensional transfer zones.

Acknowledgements

We thank Actions Marges for funding. ISTerre is part of Labex@osug2020 (ANR10 LABX56). Reviews by T. Gerya and two anonymous reviewers contributed to improve this paper.

References

Aydin, A. and Nur, A., 1982. Evolution of pull apart basins and their scale independence. *Tectonics*, **1**, 1, 91-105.

Basile, C., 2015. Transform continental margins – Part 1: concepts and models. *Tectonophysics,* **661**, 1-10. http://dx.doi.org/10.1016/j.tecto.2015.08.034

Basile C. and Brun, J.P., 1999. Transtensional faulting patterns ranging from pull-apart basins to transform continental margins: an experimental investigation. Journal of Structural *Geology*, **21**, 23-37.

Basile, C., Mascle, J. and Guiraud, R., 2005. Phanerozoic geological evolution of the Equatorial Atlantic domain. *Journal of African Earth Sciences*, **43**, 275-282.

Bellahsen, N., Leroy, S., Autin, J., Razin, P., d'Acremont, E., Sloan, H., Pik, R., Ahmed, A. and Khanbari, K., 2013. Pre-existing oblique transfer zones and transfer/transform relationships in continental margins: new insights from the southeastern Gulf of Aden, Socotra Island, Yemen. *Tectonophysics*, **607**, 32-50.

Cloos, H., 1928. Experimente zur inneren Tektonik. *Centralblatt für Mineralogie Geologie und Paläontologie*, **5**, 609-621

Dooley, T. and McClay, K., 1997. Analog modeling of pull-apart basins. *American Association of Petroleum Geologists Bulletin*, **81**, 11, 1804-1826.

Dooley, T., McClay, K. and Bonora, M., 1999. 4D evolution of segmented strike-slip fault systems: applications to NW Europe. In: *Petroleum of Northwestern Europe: Proceedings of the 5th Conference* (Fleet, A.J. and Boldy, S.A.R., Eds), 215-225, Geological Society of London, Petroleum Geology conference Series.

Dunbar, J.A., Sawyer, D.S., 1988. Continental rifting at pre-existing lithospheric weaknesses. *Nature*, **333**, 450-452.

Gerya, T., 2010. Dynamical instability produces transform faults at mid-ocean ridges. *Science*, **329**, 1047-1050.

Gerya, T., 2013a. Three-dimensional thermomechanical modeling of oceanic spreading initiation and evolution. *Physics of the Earth and Planetary Interiors*, **214**, 35-52.

Gerya, T., 2013b. Initiation of transform faults at rifted continental margins: 3D petrological-thermomechanical modeling and comparison to the Woodlark basin. *Petrology*, **21**, 6, 550-560.

Haghipour, A., 2006. Structural and kinematic map of the world. *Commission for the Geological Map of the World* – UNESCO, Paris.

Hempton, M.R. and Neher, K., 1986. Experimental fracture, strain and subsidence patterns over en échelon strike-slip faults: implications for the structural evolution of pull-apart basins. *Journal of Structural Geology*, **8**, 6, 597-605.

Hey, R. 1977. A new class of "pseudofaults" and their bearing on plate tectonics: a propagating rift model. *Earth and Planetary Science Letters*, **37**, 321-325.

Hieronymus, C.F., 2004. Control on seafloor spreading geometries by stress- and strain-induced lithospheric weakening. *Earth and Planetary Science Letters*, **222**, 177-189.

Morley, C.K., Nelson, R.A., Patton, T.L. and Munn, S.G., 1990. Transfer zones in the East African Rift System, and their relevance to hydrocarbon exploration in rifts. *American Association of Petroleum Geologists Bulletin*, **74**, 1234-1253.

Moulin, M., Aslanian, D. and Unternerh, P., 2010. A new starting point for the South and Equatorial Atlantic Ocean. *Earth Science Reviews*, **98**, 1-2, 1-37.

Mounguengui, M.M. and Guiraud, M., 2009. Neocomian to early Aptian syn-rift evolution of the normal to oblique-rifted North Gabon margin (Interior and N'Komi basins). *Marine and Petroleum Geology*, **26**, 6, 1000-1017.

Moy, D.J. and Imber, J., 2009. A critical analysis of the structure and tectonic significance of rift-oblique lineaments ('transfer zones') in the Mesozoic-Cenozoic succession of the Faroe-Shetland Basin, NE Atlantic margin. *Journal of the Geological Society*, London, **166**, 831-844.

Petrunin, A.G., Sobolev, S.V., 2008. Three-dimensional numerical models of the evolution of pull-apart basins. *Physics of the Earth and Planetary Interiors*, **171**, 387-399.

Pollard, D.D. and Aydin, A., 1984. Propagation and linkage of oceanic ridge segments. *Journal of Geophysical Research*, **89**, B12, 10017-10028.

Rahe, B., Ferril, D.A., Morris, A.P., 1998. Physical analog modeling of pull-apart evolution. *Tectonophysics*, **285**, 21-40.

Riedel, W., 1929. Zur mechanic geologischer Brucherscheinungen. *Centralblatt für Mineralogie Geologie und Paläontologie*, **B**, 354-368.

Segall, P. and Pollard, D.D., 1980. Mechanics of discontinuous faults. *Journal of Geophysical Research*, **85**, B8, 4337-4350.

Sibuet, J.C. and Mascle, J., 1978. Plate kinematic implications of Atlantic equatorial fracture zone trends. *Journal of Geophysical Research*, **83**, NB7, 3401-3421.

Taylor, B., Goodliffe, A. and Martinez, F., 2009. Initiation of transform faults at rifted continental margins. *Comptes Rendus Geoscience*, **341**, 428-438.

Tchalenko, J.S., 1970. Similarities between shear zones of different magnitudes. *Geological Society of America Bulletin*, **81**, 1625-1640.

Turcotte, D.L., 1974. Are transform faults thermal contraction cracks? *Journal of Geophysical Research*, **79**, 2573-2577.

Wilson, J.T., 1965. A new class of faults and their bearing on continental drift. *Nature*, **207**, 4995, 343-347.

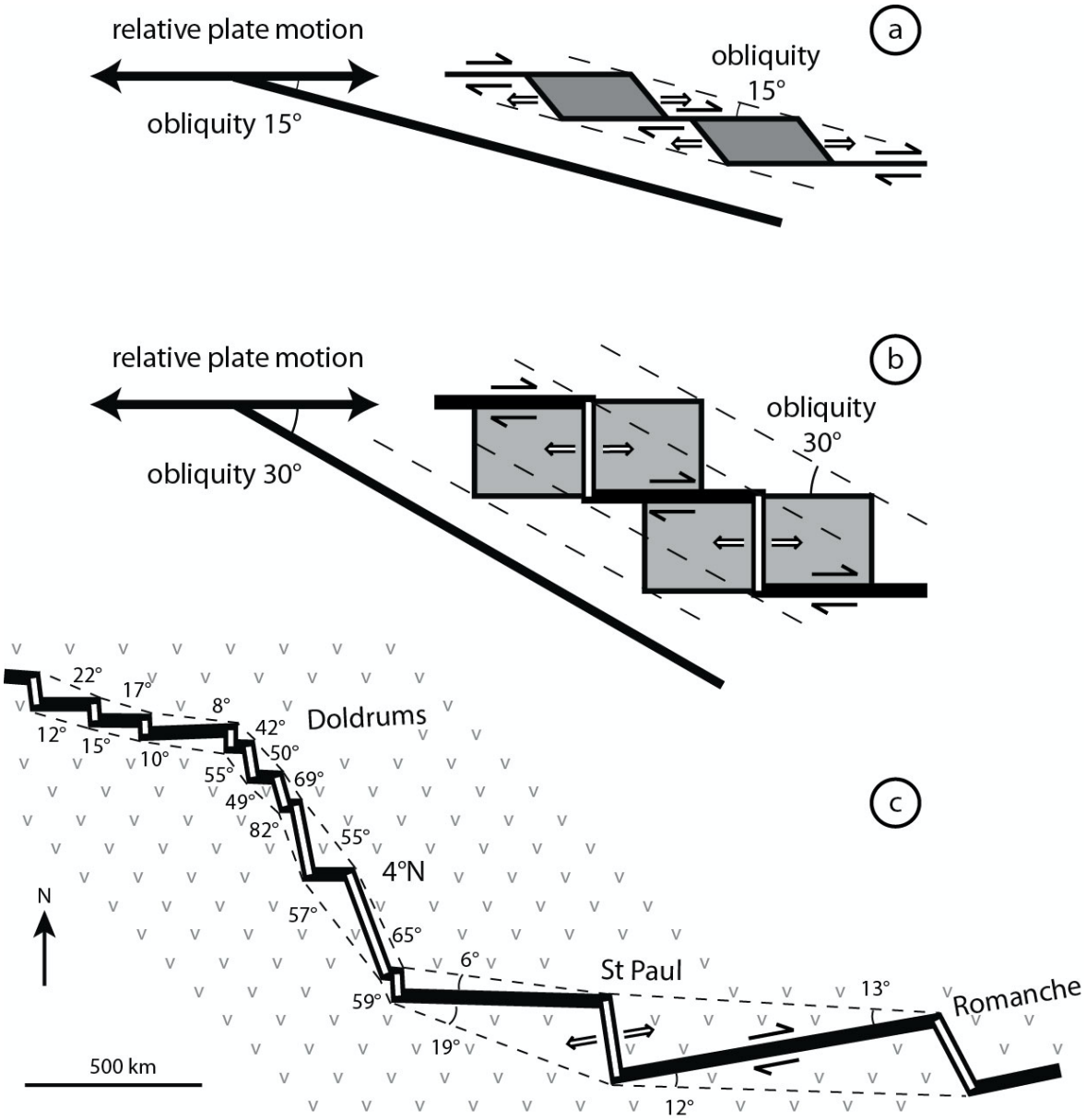

Figure 1: Kinematic partitioning in divergent setting. a: Schematic pull-apart basins (shaded) in a right-lateral step-over between en-échelon dextral strike-slip faults. No scale, the width of the basin can vary from tens of metres to several tens of kilometres (Aydin and Nur, 1982). The regional trend of the plate boundary is defined from similar transform-divergent intersections (doted lines). The obliquity is the angle between the regional trend and the relative plate motion, assumed to be parallel to the transform faults. b: obliquity for divergent continental margins (shaded areas) and oceanic accretion axis (white lines) (modified from Basile, 2015). c: schematic map of transform faults and oceanic accretion axis in the oceanic crust of the Equatorial Atlantic Ocean (modified from Haghipour, 2006). The angles indicate the obliquity measured for each transform fault.

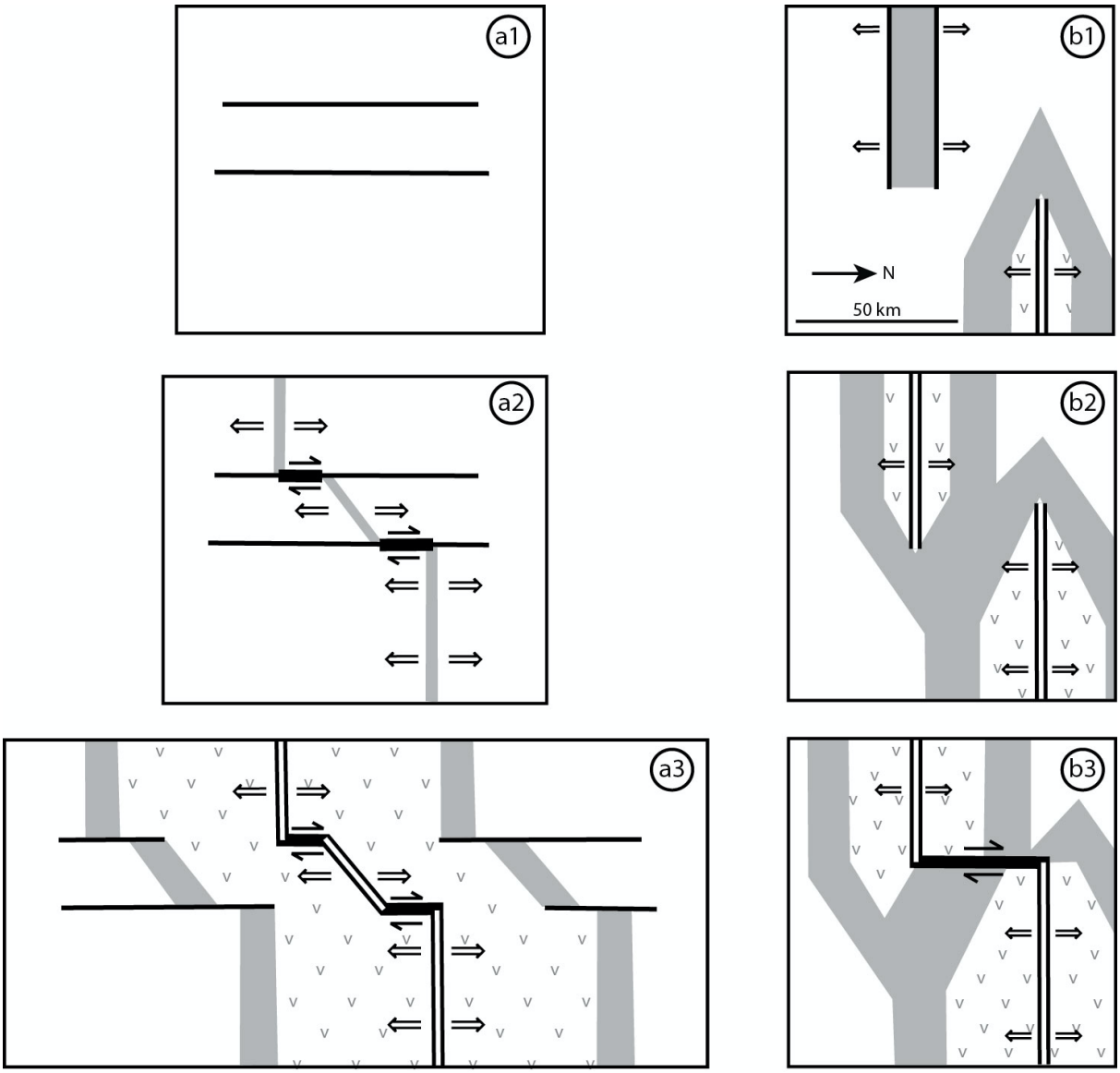

Figure 2: Two opposite conceptions for the initiation of transform faults. a : transform faults on inherited structures, modified from Wilson (1965). The three stages of the opening of an oceanic domain between two continents are a1: pre-rift, with preexisting weakness zones; a2: incipient rifting with transform faults localized on preexisting structures; a3: oceanic accretion along a plate boundary similar in shape to the previous rifted boundary (a2). No scale, but the sketch refers to the opening of the Equatorial Atlantic. b: newly formed transform fault, modified from Taylor et al. (2009). Based on the Woodlark basin example, transform fault appear (b3) by connection of propagating accretion axis (b2), but does not exist during the rifting stage (b1). White: continental or pre-rift crust; shaded: rifted crust; v indicates oceanic crust.

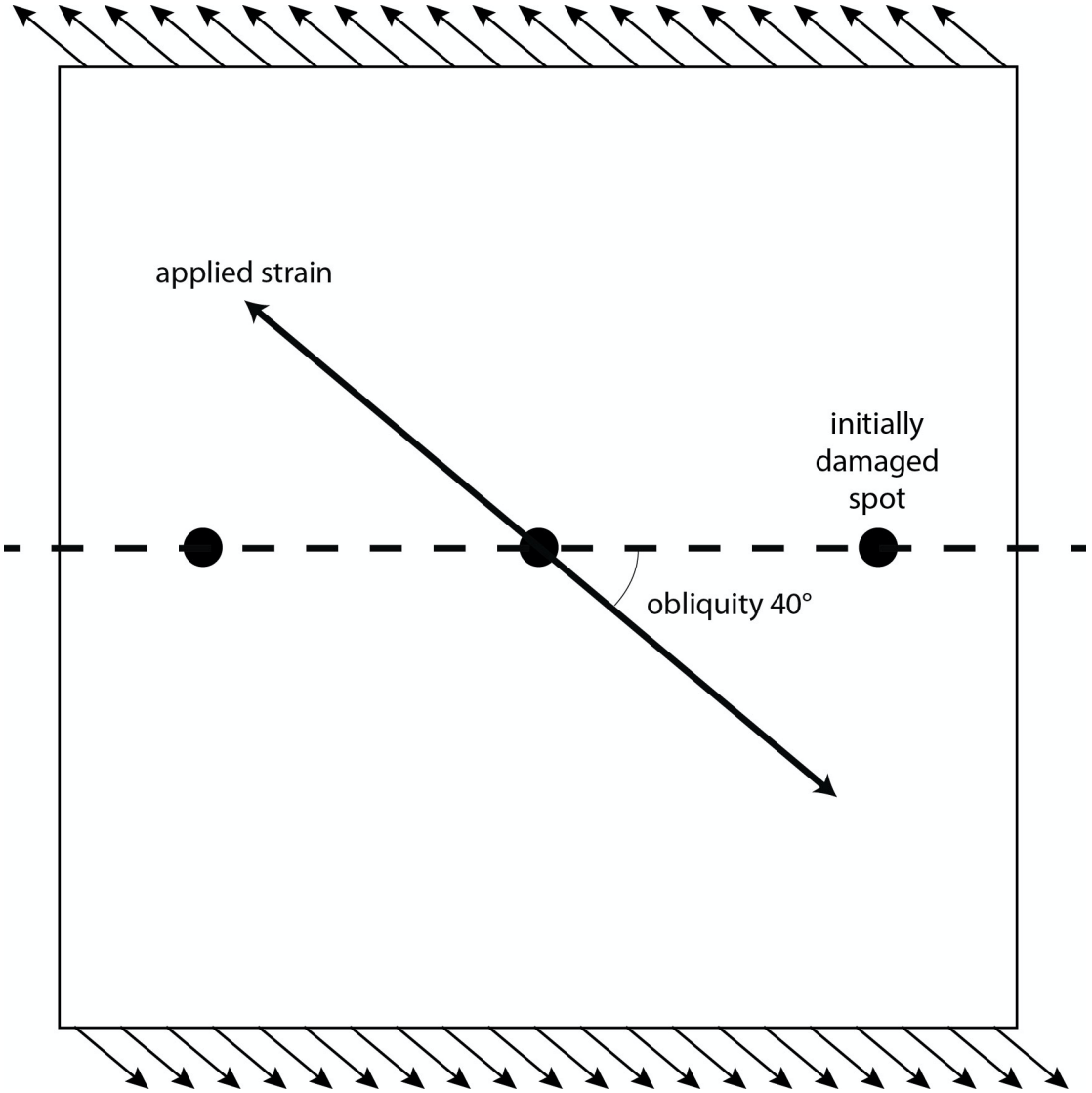

Figure 3: Map view of the experimental setup. The black dots indicate the location of the initially damaged spots in a square elastic plate. The alignment of the damaged spots (doted line) defines a 40° obliquity with the strain which is applied on the North and South borders (small arrows).

bulk modulus

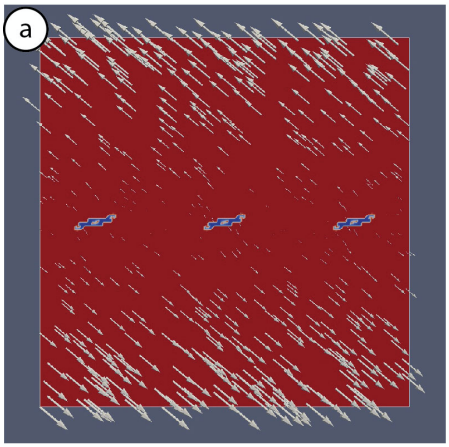

200 iterations

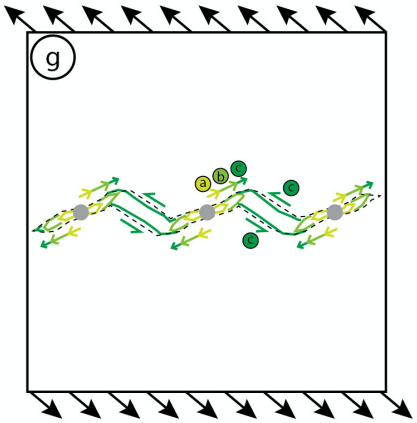

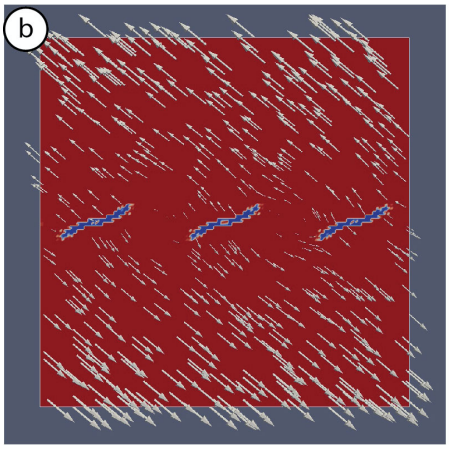

300 iterations

shear damage

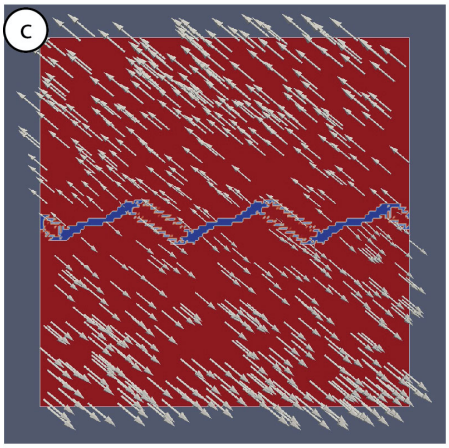

400 iterations

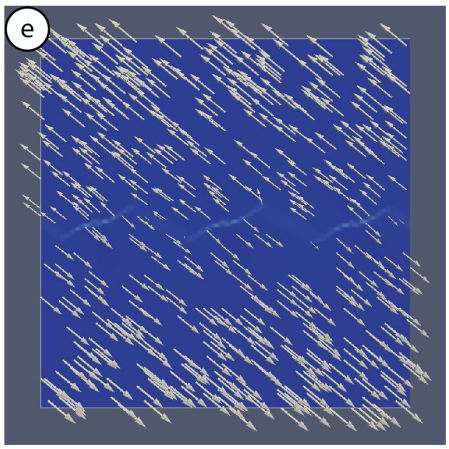

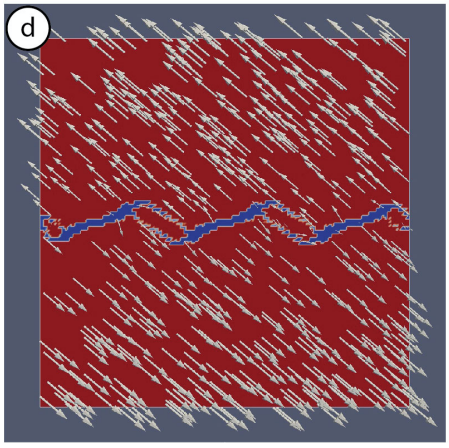

1000 iterations

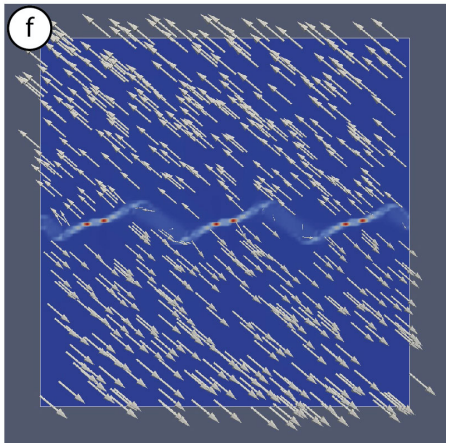

Figure 4: Successive stages of the surface of the model for 40° obliquity. From top to bottom, 200 (a), 300 (b), 400 (c and e) and 1000 (d and f) iterations. The bulk modulus is shown in the left column (a to d), where the undeformed elastic plate is in red, and the blue colors indicate the damaged areas (bulk modulus close to zero). At the bottom of the right column, the shear damage θ_2 is shown for 400 (e) and 1000 (f) iterations (undeformed in dark blue, deformed in light blue to red). The white arrows indicate the strain. They are randomly disposed for each display. g summarizes the evolution of the damaged area, from 200 iterations (a, yellow green) to 300 (b, light green) and 400 (c, dark green). The grey dots are the initially damaged spots; the dotted line represents the extension of damage area for 1000 iterations (d). See text for further comments.

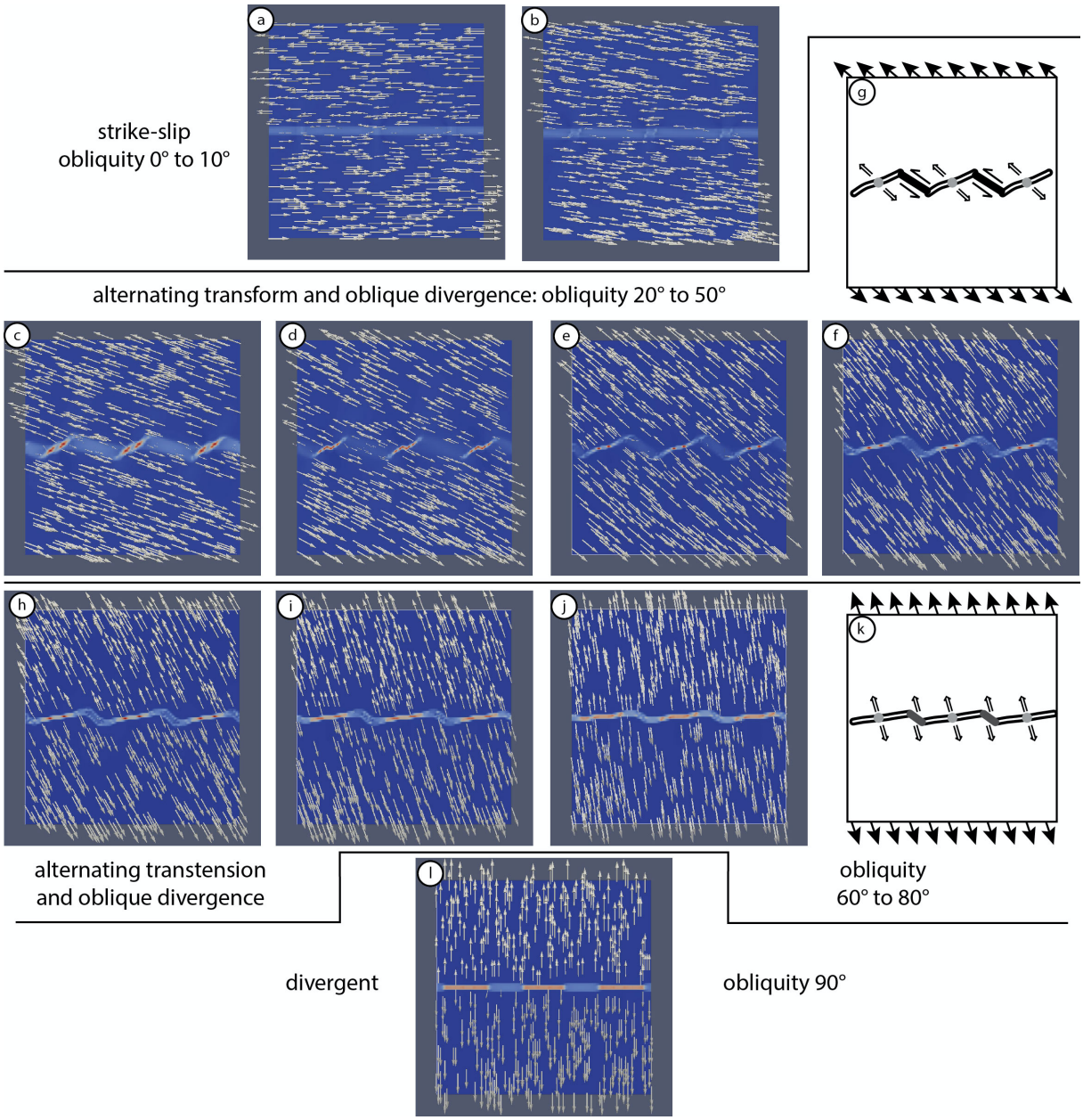

Figure 5: Shear damage (θ_2) as a function of obliquity. a: 0° obliquity, b 10°, c 20°, d 30°, e and g 40°, f 50°, h 60°, i and k 70°, j 80°, l 90°. Figures 5e and g corresponds to Figure 4f. The state of the model is shown for 1000 iterations, with the exceptions of 0° and 10 obliquity (400 iterations) and 20° obliquity (500 iterations) where the tensile strain is doubled (Table 1). The color scale (undeformed in dark blue, deformed in light blue to red) is normalized to the maximum value reached in each model. The white arrows indicate the strain, and are randomly disposed for each display. Figures 5g and 5k schematize the resulting deformation for the two types of behavior. White lines are divergent boundaries, black lines transform faults, and grey lines transfer zones. The grey dots are the initially damaged spots. See text for further comments.

Table 1: used parameters for the models, as in Hieronymus (2004). The tensile strain u_0 is doubled (2.83) for the low-obliquity models (0, 10 and 20°)

K_0	G_0	c_K	c_G	n_1	n_2	n_3	m_1	m_2	a	b	κ_1	κ_2	u_0
0.83	0.37	0.998	0.961	20	7	0	1.4	0.065	5	0.06	0.5	0.01	1.41

Supplementary material: Model description

Hieronymus (2004) assumes that the bulk (K) and shear (G) modulus depend on the damage as:

$$K = \frac{1}{2} K_0 \left\{1 - c_K \times \tanh\left(n_1\left(\theta_1 - \frac{1}{2}\right) + n_3\left(\theta_2 - \frac{1}{2}\right)\right)\right\} \quad (1)$$

$$G = \frac{1}{2} G_0 \left\{1 - c_G \times \tanh\left(n_1\left(\theta_1 - \frac{1}{2}\right) + n_2\left(\theta_2 - \frac{1}{2}\right)\right)\right\} \quad (2)$$

where K_0 and G_0 are the far-field values for the bulk and shear modulus; c_K and c_G are constants that determine the degree of elastic softening. n_1, n_2 and n_3 are parameters that control the progressive transition from the background elastic state to the maximum weakening.

Variations of tensile and shear damages are given by:

$$\frac{d\theta_1}{dt} = I_E - m_1 - \kappa_1\theta_1 \quad (3)$$

$$\frac{d\theta_2}{dt} = aII_E + bII_\sigma - m_2 - \kappa_2\theta_2 \quad (4)$$

where I_E, II_E and II_σ are the product of the first stress and strain invariants, the distortional energy, and the second invariant of the deviatoric stress, respectively; a and b are constants, m1 and m2 represent thresholds for damaging. κ_1 and κ_2 control the damage annealing.

The damage equations are coupled with the noninertial momentum equations and an elastic rheology and solved on a 101x101-node grid.

We use the same model parameter values as Hieronymus (2004) (Table 1), with the exception of parameter a, which relates shear damage θ_2 to the distortional energy in equation 4. This parameter value is increased to facilitate shear damage, and avoid healing of the damaged area. Increasing the applied tensile strain or decreasing the damage annealing constant κ_2 would yield similar results.